Photochromic reversion enables long-term tracking of single molecules in living plants.

Michelle von Arx[1]*, Kaltra Xhelilaj[1]*, Philip Schulz[2], Sven zur Oven-Krockhaus[1,3], Julien Gronnier[1#]

1. Centre for Plant Molecular Biology (ZMBP), University of Tübingen, Auf der Morgenstelle 32, 72076 Tübingen, Germany.
2. Department of Biosystems Science and Engineering, ETH Zurich, Basel, Switzerland
3. Institute for Physical and Theoretical Chemistry, University of Tübingen, 72076 Tübingen, Germany.

* These authors contributed equally to the work
# Correspondence: julien.gronnier@zmbp.uni-tuebingen.de

Abstract

Single-molecule imaging promises the observation of individual molecules at work in living cells[1,2]. In plants, however, the tracking of single molecules is generally limited to mere hundred milliseconds[3–5], making it virtually impossible to observe live dynamic cellular events with molecular resolution. Here, we introduce photochromic reversion which uses the reversion of EOS fluorescent protein's dark state upon blue light illumination[6], thereby stabilizing the fluorescent state of single molecules and extending single-molecule tracking in single particle tracking photoactivated localization microscopy (spt-PALM) experiments. Utilizing photochromic reversion, we tracked single molecules over micrometre distances for seconds. We captured transient spatial arrest events of plasma membrane proteins indicative of the observation of dynamic cellular events under physiological conditions. Finally, we implemented an analysis pipeline leveraging machine learning-based diffusional fingerprinting to automatically detect and quantify spatial arrestment, allowing precise kinetic measurements of molecular events at the nanoscale. We envision that photochromic reversion will constitute a pivotal instrument to decipher fundamental principles underlying membrane dynamics and function in plants.

Main

Our ability to comprehend fundamental principles of life is intimately linked to our capacity to observe its molecular intricacies live. Recent progress made in instrumentation and methods permits the detection, imaging, and tracking of single molecules in their native cellular environment[1,2,7,8]. Single-particle photoactivated localization microscopy (spt-PALM)[9] has been recently applied in plants and remains to date the only bona-fide single molecule tracking (SMT) approach amenable to plant samples[3–5]. Spt-PALM relies on the iterative and stochastic photo-switching or photo-conversion of fluorescent proteins (FPs) to spatially and temporally separate single molecules that can be located and tracked with nanometre precision. mEOS variants are considered the best overall performing photoconvertible FPs[8,10–12] and are the most used FP for spt-PALM experiments in plants[3–5,13–18]. mEOS variants convert irreversibly from “green” to “red” excitable spectral states upon low intensity illumination at 405 nm[10,11,19]. However, photoconverted EOS variants have been shown to enter a long-lived dark state which results from chromophore isomerization[6] (Figure 1a). Such a long-lived dark

48 state can be reverted to a fluorescent state upon illumination with 488 nm *in vitro* and animal
49 cells[6] (Figure 1b). We set to investigate the existence of a long-lived dark state of EOS-
50 translational fusions in plants. We imaged translational fusions of the plasma membrane
51 protein REMORIN1.2 (REM1.2) with mEOS2 or mEOS3.2 transiently expressed in *Nicotiana*
52 *benthamiana* using variable-angle total internal fluorescence microscopy (VA-TIRFM)[20,21].
53 Inherent to the light exposure needed for plant cultivation, we observed photo-converted
54 mEOS molecules even without 405 nm light (Supplementary Figure 1). Illumination of the
55 samples with a low amount of 488 nm light led to the appearance of additional mEOS2-
56 REM1.2 and mEOS3.2-REM1.2 molecules (Supplementary Figure 1) which rapidly disappeared
57 when the 488 nm laser was turned off (Supplementary Figure 2, Supplementary movie 1). This
58 suggests that mEOS variants enter a long-lived dark state in absence of 488 nm light. To
59 corroborate these observations, we analysed translational fusions of mEOS variants with five
60 plasma membrane proteins, REM1.2, PLASMA MEMBRANE INTRINSIC PROTEIN 2;1 (PIP2;1),
61 ARABIDOPSIS H+ ATPase 2 (AHA2), LOW TEMPERATURE INDUCED PROTEIN 6a (LTI6a) and the
62 Rho of Plant 6 (ROP6), all stably expressed in *Arabidopsis thaliana* (herein Arabidopsis). For
63 all proteins, we observed that 488 nm illumination led to the recovery of fluorescent
64 molecules (Supplementary Figure 3). Exposition to different light intensities indicates that
65 approximately 10 µW at the sample plane is sufficient to recover half of the dark state mEOS
66 molecules (Supplementary Figure 4). In transient assays we observed that upon 488 nm
67 illumination, single molecules continuously emit light while they seem to cycle between
68 fluorescent and dark states in its absence (Supplementary Figure 2, Supplementary Movie 1).
69 Intermittent application of 488 nm light on seedlings expressing the relatively static PIP2;1-
70 mEOS further suggests that the disappearance of fluorescent molecules is due to the re-entry
71 into the long-lived dark state as molecules can be recovered at the same position during a
72 second application of 488nm light (Supplementary Figure 5). Altogether, these observations
73 indicate that photo-converted mEOS molecules are predominantly in a non-fluorescent dark
74 state and continuously cycle between fluorescent and a long-lived dark state when expressed
75 in plants. These observations also indicate that, due to the cycling between long-lived dark
76 and fluorescent states, the same molecules may be counted several times as independent
77 molecules in classical PALM experiments. The application of 488 nm light was shown to
78 reduce tracks interruption[6], and we observed that continuous 488 nm application maintains
79 mEOS molecules in a fluorescent state (Supplementary Movie 1, Supplementary Movie 2)
80 which we further explored quantitatively. By comparing the track duration of single molecules
81 in presence and absence of 488 nm light exposure we observed that continuous illumination
82 with 488 nm light increased the duration of single-molecule tracks (Supplementary Figure 6-
83 8) without affecting computed instantaneous diffusion coefficients (Supplementary Figure 9).
84 Furthermore, we observed that continuous 488 nm illumination effectively prolonged the
85 duration of tracks independently of the mEOS variants, the expression conditions, or the
86 mobility behaviour of the protein tested (Supplementary Figure 6-8, Supplementary Figure
87 10). In these experiments, we tracked molecules that were previously photo-converted and
88 excited due to ambient and imaging conditions. Since fluorescent proteins emit a finite
89 number of photons before photobleaching[7], we reasoned that we could track newly photo-
90 converted molecules longer. We thus performed single molecule tracking experiments upon
91 low irradiation with 405 nm laser illumination to induce mEOS photo-conversion, in absence
92 and presence of 488 nm illumination. Under these imaging conditions (Figure 1c) we observed
93 an additional increase in the proportion of long single molecule tracks (longer than 5 seconds)
94 representing approximately 15% of all tracks (Supplementary Figure 11) upon 488 nm

illumination. Various imaging modalities have previously shown that the plasma membrane is laterally organized into nanodomains[22–28], which are proposed to provide means for dynamic spatial and temporal regulation of molecular events. However, the dynamic nature of plasma membrane nano-organization has never been directly experimentally assessed in plants. In our experiments we repetitively captured transient events of spatiotemporal arrests of tested proteins and observed live molecules entries and exits from defined membrane nano-environments (Figure 1d), indicative of the observation of cellular events under physiological conditions. To gain quantitative information on these events, we developed an analysis pipeline based on single-particle diffusional fingerprinting (Figure 2a)[29], which we adapted to discriminate transient spatiotemporal arrest within single molecule tracks (see method section). In brief, we considered twenty-one features, such as step lengths, diffusion coefficient and local kernel density of localization to predict changes in diffusional state within single molecule tracks. Utilizing our pipeline, we automatically detected changes in diffusional behaviour for all tested proteins (Figure 2b-c) and computed the frequency of these events, their duration, and the corresponding area (Figure 2c). We detected changes in molecular motion which could not be inferred from bulk analysis of the diffusion coefficient (Figure 2c, Supplementary Figure 10). We envision that the approach implemented herein will constitute a pivotal instrument to uncover many fundamental functional aspects of the plasma membrane. Indeed, the precise kinetic measurements of membrane-based events now made accessible will open new possibilities to unveil how membrane nanodomains are form and maintained, to dissect potential links between membrane dynamics and signaling, as well as to finely characterised the interplay between the molecular components constituting the cell surface continuum. We foresee that the application of this imaging modality can be extended to other cellular environments and processes such as transcription[30,31] and organelle communication[32].

Acknowledgement

We thank Alexandre Martinière for providing seeds of the transgenic lines Col-0/pUb::mEOS2-AHA2, Col-0/pPIP2;1::PIP2;1-mEOS2, Col-0/pUb::mEOS2-ROP6 and Col-0/pUb::Lti6a-mEOS2. We thank Thomas Ott and Sébastien Mongrand for sharing seeds of the transgenic line *rem1.2/rem1.3/rem1.4*. We thank Yvon Jaillais, Alexandre Martinière, Vincent Bayle and Dominique Bourgeois for comments on the manuscript. We thank all members of the NanoSignaling Lab for fruitful discussion and feedback on the manuscript.

Funding

This work was supported by the German Research Foundation (DFG) grants SFB1101 (A09) and TRR356 (B01) to J.G, and SFB1101 grant (Z02) supporting S.z.O.-K. We also thank the DFG for the grants FUGG: INST 37/991-1, INST 37/819-1, INST 37/965-1 supporting the acquisition of scientific equipment.

FIGURE LEGENDS

Figure 1 | Photochromic reversion enables long-term single-molecule tracking.
a. AlphaFold2 predicted structure of the fluorescent protein mEOS3.2 in which the beta barrel body is depicted in blue and the chromophore in pink.
b. Photochromic transitions of mEOS chromophore. mEOS molecules are photoconverted using 405 nm light, excited using 561 nm light and spontaneously cycles between excited-fluorescent (red) and excited-dark state. They can be maintained in an excited-fluorescent state using 488 nm light.
c. Illustration of the illumination conditions used for long-term single-molecule tracking.
d. Examples of single-molecules tracks obtained using photochromic recovery in the stable *Arabidopsis* transgenic plants, Col-0/pUb10::Lti6a-mEOS2 Col-0/pUb::mEOS2-AHA2, Col-0/pPIP2;1::PIP2;1-mEOS2, Col-0/pUb::mEOS2-ROP6, and *rem1.2/rem1.3/rem1.4*/ pREM1.2::mEOS3.2-REM1.2. Imaging was performed in five-day-old seedlings cotyledon epidermal cells in presence of continuous 488 nm (25 µW) and continuous 561 nm (1000 µW), and in presence of pulsed 405 nm (2 µW) light exposure.

Figure 2 | Analysis of transient spatial arrest events of plasma membrane proteins.
a. Schematic depiction of machine-learning based diffusional fingerprinting. A combination of diffusional state and motion behaviour parameters serve as a bases to define a spatiotemporal signature which is used to automatically predict spatial arrest of diffusion (SAD) within single-molecule tracks.
b. Examples of track segmentations using diffusional fingerprinting on long-term single-molecule tracks observed in the stable *Arabidopsis* transgenic plants Col-0/pUb10::Lti6a-mEOS2, Col-0/pUb::mEOS2-AHA2, Col-0/pPIP2;1::PIP2;1-mEOS2, Col-0/pUb::mEOS2-ROP6, and *rem1.2/rem1.3/rem1.4*/pREM1.2::mEOS3.2-REM1.2. Imaging was performed in five-day-old seedlings cotyledon epidermal cells in in presence of continuous 488 nm (25 µW) and continuous 561 nm (1000 µW), and in presence of pulsed 405 nm (2 µW) light exposure. Tracks segments predicted as transient SAD are indicated in green.
c. Quantitative analysis of the frequency of SAD events per track (left) their duration (middle) and the area in which molecule were SAD (right). Graphs are boxplots, scattered data points indicate average values obtained from individual cells. Total number of cells (n) analysed equal 9 for Lti6a-mEOS2, n=10 for mEOS2-AHA2, n=7 for mEOS2-ROP6, n=5 for PIP2;1-mEOS2 and n=7 for mEOS3.2-REM1.2. Conditions which do not share a letter are significantly different in Wilcoxon rank sum test ($p<0.005$).

Supplementary Figure 1 | Effect of 488nm illumination on mEOS2-REM1.2 and mEOS3.2-REM1.2 molecules transiently expressed in *N. benthamiana*.
Quantification of the number of molecules observed and of their fluorescence intensity before (t) and upon 488 nm light exposure (t + 100ms) for mEOS-REM1.2 (**a**) and mEOS3.2-REM1.2 (**b**) molecules transiently expressed in N. benthamiana 30 hours post infiltration, in presence of continuous 561 nm (1000 µW) and absence of 405 nm light exposure. Each dot represents the average value observed for individual cells. The lines connect values observed for the same cell before and upon 488 nm laser application. P values report two-tailed Mann-Whitney statistical test.

Supplementary Figure 2 | Single molecules rapidly return to a dark state in absence of 488 nm illumination.

Images correspond to individual time frames of mEOS3.2-REM1.2 molecules observed upon transient expression in *N. benthamiana*, in presence or absence of 488 nm (25 µW) in presence continuous 561 nm (1000 µW) and in absence of 405 nm light exposure.
See the corresponding supplementary movie 1.

Supplementary Figure 3 | Effect of 488nm illumination on five plasma membrane-localized mEOS translational fusions expressed in *Arabidopsis thaliana*.

Quantification of the number of molecules observed before (t) and upon 488 nm light exposure (t + 100ms) for Lti6a-mEOS2 (**a**) mEOS2-AHA2 (**b**), mEOS3.2-REM1.2 (**c**), mEOS2-ROP6 (**d**), and PIP2;1-mEOS2 (**e**) in five-days-old Arabidopsis cotyledon epidermal cells, in presence continuous 561 nm (1000 µW) and in absence of 405 nm light exposure. Each dot represents the average value observed for individual cells expressed as relative to the control condition (- 488 nm light application). The lines connect values observed for the same cell before and after 488 nm laser application. Total number of cells (n) analysed equal 7 for Lti6a-mEOS2 n=7 for mEOS2-AHA2, n=5 for mEOS3.2-REM1.2, n=6 for mEOS2-ROP6, and n=7 PIP2;1-mEOS2. P values report two-tailed Mann-Whitney statistical test.

Supplementary Figure 4 | Analysis of the dose response to 488 nm light exposure.

Quantification of the number of mEOS3.2-REM1.2 (**a-b**) and mEOS2-AHA2 (**c-d**) molecules observed before and upon exposure to 488 nm light of several intensities in five-days-old Arabidopsis epidermal cells, in presence continuous 561 nm (1000 µW) and in absence of 405 nm light exposure. In **a** and **c**, each dot represents the average value observed for individual cells expressed as relative to the control condition (- 488 nm light application). The lines connect values observed for the same cell before and upon 488 nm laser application. P values report two-tailed Mann-Whitney statistical test. The graphs in (**b**) and (**d**) depict the number of observed molecules as a function of 488 nm light intensity. Data point represent average values observed across cells for each light intensity conditions ± standard error to the mean. Red curves represent non-linear fit of the data. Total number of cells (n) analysed equal 28 for mEOS3.2-REM1.2 and n=29 for mEOS2-AHA2.

Supplementary Figure 5 | Sequential exposure to 488 nm shows controlled cycling of photo-converted mEOS molecules between fluorescent and dark state.

Analysis of PIP2;1-mEOS2 fluorescence overtime in five-days-old Arabidopsis epidermal cells in presence and absence of continuous 488 nm (25 µW), in presence continuous 561 nm (1000 µW) and in absence of 405 nm light exposure.
a. The image corresponds to a projection of the fluorescence observed across x and y coordinates into a single plane (coordinate x) overtime.
b. Each image corresponds to individual time frames (x,y) of the temporal projection depicted in A.

Supplementary Figure 6 | Effect of 488 nm light exposure on trajectories duration of mEOS2-REM1.2 and mEOS3.2-REM1.2 transiently expressed in *N. benthamiana.*

a and **d** show representative images of single-molecule trajectories of mEOS2-REM1.2 (**A**) and mEOS3.2 (**d**) observed in 3 weeks old *N. benthamiana* leaf epidermal cells in presence and

227 absence of continuous 488 nm (25 µW), in presence of continuous 561 nm (1000 µW) and in
228 absence of 405 nm light exposure. Trajectories are coloured based on their duration.
229 **b** and **e**. Graphs depict trajectories duration for individual mEOS2-REM1.2 (**b**) and mEOS3.2
230 (**e**) tracks in presence and absence of continuous 488 nm (25 µW), in presence of continuous
231 561 nm (1000 µW) and in absence of 405 nm light exposure. P values report two-tailed Mann-
232 Whitney statistical test.
233 **c** and **f**. Graphs correspond to normalized histogram of trajectories duration observed in
234 presence and absence of continuous 488 nm (25 µW), in presence of continuous 561 nm
235 (1000 µW) and in absence of 405 nm light exposure for mEOS2-REM1.2 (**C**) and mEOS3.2-
236 REM1.2 (**F**). Percentages indicate the proportion of trajectories whose duration is equal or
237 longer than 5 seconds. Total number of cells (n) analysed equal 25 for mEOS2-REM1.2, n=32
238 for mEOS3.2-REM1.2 from two independent experiments.
239
240 **Supplementary Figure 7 | Effect of 488 nm light intensity on trajectories duration of mEOS2-**
241 **AHA2 and mEOS3.2-REM1.2.**
242 **a-b**. Graphs correspond to normalized histogram of trajectories duration (s) observed upon
243 different intensity of 488 nm light exposure for mEOS2-AHA2 (**A**) and mEOS3.2-REM1.2 (**B**).
244 Percentages indicate the proportion of trajectories whose duration is equal or longer than 5
245 seconds. Total number of cells (n) analysed equal 35 for mEOS3.2-REM1.2 and n=38 for
246 mEOS2-AHA2 collected in one experiment.
247 **c**. Representative images of single-molecule trajectories of mEOS2-AHA2 (left) and mEOS3.2-
248 REM1.2 (right). Trajectories are coloured based on their duration.
249
250 **Supplementary Figure 8 | Effect of 488 nm light exposure on trajectories duration of Lti6a-**
251 **mEOS2, mEOS2-ROP6 and PIP2;1-mEOS2.**
252 **a**, **d** and **g** show representative images of single molecule trajectories of Lti6a-mEOS2 (**A**),
253 mEOS2-ROP6 (**d**) and PIP2;1-mEOS2 (**g**) observed in five-days-old Arabidopsis epidermal cells
254 in presence and absence of continuous 488 nm (25 µW), in presence of continuous 561 nm
255 (1000 µW) and absence of 405 nm light exposure. Trajectories are coloured based on their
256 duration.
257 **b**, **e** and **h**. Graphs depict trajectories duration for individual tracks of Lti6a-mEOS2 (**B**),
258 mEOS2-ROP6 (**E**) and PIP2;1-mEOS2 (**H**) in presence and absence of continuous 488 nm light
259 exposure (25 µW), in presence of continuous 561 nm (1000 µW) and in absence of 405 nm
260 light exposure. P values report two-tailed Mann-Whitney statistical test.
261 **c**, **f** and **i**. Graphs correspond to normalized histogram of trajectories duration observed in
262 presence and absence of continuous 488 nm light exposure (25 µW) for Lti6a-mEOS2 (**C**),
263 mEOS2-ROP6 (**F**) and PIP2;1-mEOS2 (**I**). Percentages indicate the proportion of trajectories
264 which duration is superior or equal to 5 seconds. Total number of cells (n) analysed equal 18
265 for Lti6a-mEOS2, n=12 for mEOS2-ROP6 and n=11 for PIP2;1-mEOS2 from two independent
266 experiments.
267
268 **Supplementary Figure 9 | 488 nm light exposure does not affect diffusion coefficient.**
269 Analysis of the diffusion coefficient (D) of mEOS3.2-REM1.2 (**a-c**) and mEOS2-AHA2 (**b-c**) upon
270 exposure of five-days-old Arabidopsis epidermal cells with different 488 nm light intensities.
271 **A** and **B** depict the distribution of mEOS3.2-REM1.2 and mEOS2-AHA2 molecules according to
272 their apparent diffusion coefficient. **c** and **d** represent the average diffusion coefficient for
273 individual cells. Total number of cells (n) analysed equal 35 for mEOS3.2-REM1.2 and n=38 for

mEOS2-AHA2 collected in one experiment, pink crosses indicate mean ± s.e.m. Conditions sharing a letter are not significantly different in Dunn's multiple comparison test (P>0.22).

Supplementary Figure 10 | Analysis of the apparent diffusion coefficient of plasma membrane proteins used in this study.

The graph represents the distribution of mEOS2-AHA2, PIP2;1-mEOS2, mEOS3.2-REM1.2, mEOS2-ROP6 and Lti6a-mEOS2 molecules, observed in five-days-old Arabidopsis epidermal cells, according to their apparent diffusion coefficient. Total number of cells (n) analysed equal 12 for mEOS2-AHA2, n=11 PIP2;1-mEOS2, n=19 for mEOS3.2-REM1.2, n=9 for mEOS2-ROP6 and n=11 for Lti6a-mEOS2, from two independent experiments.

Supplementary Figure 11 | Analysis of trajectory duration of newly photo-converted molecules.

A. Representative images of single-molecule trajectories of mEOS3.2-REM1.2 observed in five-days-old Arabidopsis epidermal cells in presence and absence of continuous 488 nm light (25 µW), in presence of continuous 561 nm (1000 µW) and pulsed 405 nm (2 µW) light exposure. Scale bar indicate 2 µm.

B. Graph depicts trajectories duration for individual tracks mEOS3.2-REM1.2 in presence and absence of continuous 488 nm light exposure (25 µW). P values report two-tailed Mann-Whitney statistical test.

C. Graphs correspond to normalized histogram of trajectories duration observed in presence and absence of continuous 488 nm light exposure (25 µW) for mEOS3.2-REM1.2. Percentages indicate the proportion of trajectories whose duration is equal or longer than 5 seconds. Total number of cells (n) analysed equal 18 from two independent experiments.

Supplementary Movie 1 | Effect of 488 nm illumination in mEOS3.2-REM1.2 fluorescence behaviour.

Observation of 3-week-old *Nicotiana benthamiana* leaves transiently transformed with pUb10::mEOS3.2-REM1.2 and imaged in presence (488 on) and absence of 488 nm (25 µW), continuous 561 nm (1000 µW) and without 405 nm light exposure. Scale bar indicate 2 µm.

Supplementary Movie 2 | Long-term tracking of mEOS3.2-REM1.2 in Arabidopsis cotyledon epidermal cells.

Five-day-old seedlings of *rem1.2*/*rem1.*3/*rem1.4*/pREM1.2::mEOS3.2-REM1.2 were imaged in presence of continuous 488 nm (25 µW), continuous 561 nm (1000 µW) and pulsed 405 nm (2 µW) light exposure. Scale bar indicate 2 µm.

Supplementary Table 1 | List of primers used in this study.

312 **MATERIAL AND METHODS**
313
314 **Plant materials and culture.**
315 All stable transgenic plants used in this work were Arabidopsis thaliana L. (Heyn.), accession
316 Columbia 0. Seeds were stratified at 4°C for 2 days and germinated on half strength Murashige
317 and Skoog (½ MS) medium supplemented with sucrose (10 $g.L^{-1}$) and agar (8 $g.L^{-1}$)[33] and grown
318 in chambers under control conditions with 70 % relative humidity and cycles of 16 h of light
319 (~150 µE m^{-2} sec^{-1}) and 8 h of dark at 21 °C. The Arabidopsis transgenic lines Col-
320 0/pUb::mEOS2-AHA2[34], Col-0/pPIP2;1::PIP2;1- mEOS2, Col-0/pUb::Lti6a-mEOS2[3] and Col-
321 0/pUb::mEOS2-ROP6[15], were previously described. The
322 *rem1.2/rem1.3/rem1.4/*pREM1.2::mEOS3.2-REM1.2 line was generating by transforming the
323 *rem1.2/rem1.3/rem1.4* T-DNA mutant line [17,35] with pREM1.2::mEOS3.2-REM1.2 plasmid
324 using floral dipping[36]. 3-weeks-old Nicotiana benthamiana leaves were transiently
325 transformed using solution (OD_{600}=0.1) of *Agrobacterium tumefaciens* strain GV3101 carrying
326 corresponding constructs as previously described[37].
327
328 **Molecular cloning.**
329 The REM1.2 coding sequence was amplified using Arabidopsis Col-0 complementary DNA
330 (cDNA) and the native promoter of REM1.2 (pREM1.2) was amplified using Arabidopsis Col-0
331 genomic DNA (gDNA) as templates and the primers listed in the Supplementary Table 1. Both
332 sequences were inserted into a pUC57-based LVL1 golden gate plasmid[38] by blunt-end
333 cloning. The codon-optimized coding sequences of mEOS2 and mEOS3.2 were synthetized as
334 gene fragment by TwistBioscience and cloned into a pUC57-based LVL1 golden gate plasmid[38],
335 position B-C, using the type II restriction enzyme BpiI. The resulting constructs were used to
336 generate Xpre2-S (pCAMBIA) binary LVL2 plasmids encoding for REM1.2 N-terminally tagged
337 with mEOS variants under the control of the UBQ10 promoter (pUb) or native promoter
338 (pUb::mEOS2-REM1.2, pUb::mEOS3.2-REM1.2 or pREM1.2::mEOS3.2-REM1.2). All constructs
339 were verified by sanger sequencing. The binary vectors were transferred into *Agrobacterium*
340 *tumefaciens* strain GV3101 for flower dip transformation of Arabidopsis[36] or transient
341 transformation of *Nicotiana benthamiana* leaves.
342
343 **Variable angle-total internal reflection microscopy (VA-TIRFM)**
344 VA-TIRM imaging was operated on a custom-build TIRFM set-up[18], equipped with an 100x
345 objective NA 1.49 (Zeiss, 421190-9800-000), four laser lines (405, 488, 561 and 642 nm), a
346 polychromatic modulator (AOTF, AA OPTO-ELECTRONIC) and a sCMOS camera (Hamamatsu
347 Photonics, ORCA-Flash4.0 V2). To ensure that the target laser power value always
348 corresponds to the actual irradiance in the sample plane, the power of each laser line was
349 calibrated before each experiment using a PM100D detector (Thorlabs). Arabidopsis five-
350 days-old seedlings or leaf discs (4 mm in diameter) of 3-weeks-old *N. benthamiana* leaves (28
351 to 34 hours post agrobacterium infiltration) were mounted between two coverslips (Epredia
352 24x50 mm #1) in liquid ½ MS medium and delicately placed on the specimen stage without
353 additional weight. Images were acquired at 20 Hz frame rate, using 1000 µW 561nm laser
354 power, with or without 2 µW 405 nm laser power and with or without 1-30 µW 488 nm laser
355 power. The emitted light was filtered using 568 LP Edge Basic Long-pass Filter, 584/40 ET
356 Band-pass filters (AHF analysentechnik AG) and recorded from a 51.2 x 51.2 µm region of
357 interest, 100 nm pixel size.
358

Single-particle tracking photoactivated localization microscopy (spt-PALM)

To ensure bona-fide single-molecule tracking we analysed frames with relatively low molecule density (ca. 0.1 – 1 molecule per μm^2). We used the plugin TrackMate7[39] in Fiji[40] to reconstruct single molecule trajectories. Single particles were segmented frame-by-frame by applying a Laplacian of Gaussian (LoG) filter and estimated particle size of 0.3 µm. Individual single particles were localized with sub-pixel resolution using a built-in quadratic fitting scheme. Single-particle trajectories were reconstructed using a simple linear assignment problem [41] with a maximal linking distance of 0.4 µm and a 4 frames-gap-closing maximum. The coordinates of the single particle trajectories were then further analysed using a custom-made python script to calculate the mean square displacement (MSD) and diffusion coefficient (D) in batch mode. Only tracks with a minimum of five localizations were kept for analysis. The MSD and diffusion coefficient was calculated based on the first four time points of each trajectory as previously described[42].

Analysis of transient spatiotemporal arrest of lateral diffusion.

The transient spatial arrest of individual molecules was analysed using a custom-made pipeline based on the previously published diffusional fingerprinting method[29]. Briefly, we used a pretrained Hidden Markov Model (HMM) to estimate time in states t0-t3, where t0 = time in confined state, t1= time in sub diffusive state, t2 = time in normal diffusive state and t3 = time in super diffusive state[29]. However, instead of using the average time spend in respective states per track, we extracted the estimated states for each time step per track for all tracks. To obtain estimations of the state for confined and diffusive only, we simplified the four states into two (t0=t1=0, t2=t3=1), and defined 0 = confined and 1 = unconfined. Further, we consider state changes only in the case of 12 consecutive confined steps. In addition, we implemented four additional criteria, which we defined empirically, to maximize the robustness and versatility with which changes in diffusional states are captured. First, since spatially arrested molecules tend to have shorter motion steps (x,y) between consecutive time points, we excluded potential confinements with step lengths > 0.09 µm in 4 consecutive steps. Secondly, we considered that when spatially arrested, the angle of the track connecting successive localization is smaller for confined molecule than for diffusive molecules. We thus calculated the angles of consecutive steps and accepted confined steps only if the sum of angles of 10 consecutive steps does not exceed 600°. As previously shown[43], a 2-dimensional Kernel density estimation (KDE) can be used to calculate the density of points and reveal local increase in the number of single molecule localization. Thus, as a third criterion we considered variation in KDE for each track. To obtain a binary classification based on KDE, we categorized KDE values into 9 equal bins, inverted the counts and accepted possible spatial arrestment only if the sum of 10 consecutive tracks does not exceed 13. Fourth, we considered that when a molecule is spatially arrested it is more prone to intersect itself at these locations. We therefore computed the self-intersections of each track using a sliding window (*i.e.,* n=1 with n=4, 5, 6 and 7; n=2 with n=5, 6, 7 and 8, etc.). We next considered spatial arrest events if the tracks were intersecting at least 6 times within 10 consecutive steps. Finally, we voted on the spatial arrest predictions of all 5 calculated features (diffusional fingerprint, step length, angles, KDE, intersections) and only accepted steps spatial arrest events if at least 3 features predicted the steps as arrested. From the localisations of predicted spatial arrest events, we then calculated a convex hull and subsequently assigned all points inside the hull to the category “arrested”. At the end of the workflow, the pipeline creates a data frame storing for each track the parameters of the diffusional fingerprinting[29], the time spent in both arrested

and non-arrested state, the number of time points per predicted spatial arrest event, the convex hull area of the predicted arrestment, as well as the number of predicted spatial arrest per track.

Statistical analysis

The number of independent experiments and the number of individual cells analysed per condition and collected across these experiments are indicated in each figure legends. The statical tests used are reported in the figure legends and have been performed using R or GraphPad Prism.

REFERENCES

1. Kusumi, A., Tsunoyama, T. A., Hirosawa, K. M., Kasai, R. S. & Fujiwara, T. K. Tracking single molecules at work in living cells. *Nature Publishing Group* **10**, 524–532 (2014).
2. Lelek, M. *et al.* Single-molecule localization microscopy. *Nature Reviews Methods Primers 2021 1:1* **1**, 1–27 (2021).
3. Hosy, E. *et al.* Super-Resolved and Dynamic Imaging of Membrane Proteins in Plant Cells Reveal Contrasting Kinetic Profiles and Multiple Confinement Mechanisms. *Mol Plant* **8**, 339–342 (2015).
4. Gronnier, J. *et al.* Structural basis for plant plasma membrane protein dynamics and organization into functional nanodomains. *Elife* **6**, 1–24 (2017).
5. Bayle, V. *et al.* Single-particle tracking photoactivated localization microscopy of membrane proteins in living plant tissues. *Nature Protocols 2021 16:3* **16**, 1600–1628 (2021).
6. De Zitter, E. *et al.* Mechanistic investigation of mEos4b reveals a strategy to reduce track interruptions in sptPALM. *Nature Methods 2019 16:8* **16**, 707–710 (2019).
7. Nguyen, T. D., Chen, Y. I., Chen, L. H. & Yeh, H. C. Recent Advances in Single-Molecule Tracking and Imaging Techniques. **16**, 253–284 (2023).
8. Rodriguez, E. A. *et al.* The Growing and Glowing Toolbox of Fluorescent and Photoactive Proteins. *Trends Biochem Sci* **42**, 111–129 (2017).
9. Manley, S. *et al.* High-density mapping of single-molecule trajectories with photoactivated localization microscopy. *Nat Methods* **5**, 155–157 (2008).
10. Wang, S., Moffitt, J. R., Dempsey, G. T., Xie, X. S. & Zhuang, X. Characterization and development of photoactivatable fluorescent proteins for single-molecule-based superresolution imaging. *Proc Natl Acad Sci U S A* **111**, 8452–8457 (2014).
11. McKinney, S. A., Murphy, C. S., Hazelwood, K. L., Davidson, M. W. & Looger, L. L. A bright and photostable photoconvertible fluorescent protein. *Nature Methods 2009 6:2* **6**, 131–133 (2009).
12. Zhang, M. *et al.* Rational design of true monomeric and bright photoactivatable fluorescent proteins. **9**, 727–729 (2012).
13. Perraki, A. *et al.* REM1.3's phospho-status defines its plasma membrane nanodomain organization and activity in restricting PVX cell-to-cell movement. *PLoS Pathog* **14**, e1007378 (2018).
14. Smokvarska, M. *et al.* A Plasma Membrane Nanodomain Ensures Signal Specificity during Osmotic Signaling in Plants. *Current Biology* **30**, 4654-4664.e4 (2020).
15. Platre, M. P. *et al.* Developmental control of plant Rho GTPase nano-organization by the lipid phosphatidylserine. *Science (1979)* **364**, 57–62 (2019).
16. Smokvarska, M. *et al.* The receptor kinase FERONIA regulates phosphatidylserine localization at the cell surface to modulate ROP signaling. *Sci Adv* **9**, (2023).
17. Jolivet, M.-D. *et al.* Interdependence of a kinase and its cognate substrate plasma membrane nanoscale dynamics underlies Arabidopsis response to viral infection. *bioRxiv* 2023.07.31.551174 (2023) doi:10.1101/2023.07.31.551174.

18. Rohr, L. *et al.* OneFlowTraX: A User-Friendly Software for Super-Resolution Analysis of Single-Molecule Dynamics and Nanoscale Organization. *bioRxiv* 2023.08.10.552827 (2023) doi:10.1101/2023.08.10.552827.
19. Wulffele, J., Thédié, D., Glushonkov, O. & Bourgeois, D. MEos4b Photoconversion Efficiency Depends on Laser Illumination Conditions Used in PALM. *Journal of Physical Chemistry Letters* **13**, 5075–5080 (2022).
20. Tokunaga, M., Imamoto, N. & Sakata-Sogawa, K. Highly inclined thin illumination enables clear single-molecule imaging in cells. *Nat Methods* **5**, 159–161 (2008).
21. Konopka, C. A. & Bednarek, S. Y. Variable-angle epifluorescence microscopy: A new way to look at protein dynamics in the plant cell cortex. *Plant Journal* **53**, 186–196 (2008).
22. Raffaele, S. *et al.* Remorin, a solanaceae protein resident in membrane rafts and plasmodesmata, impairs potato virus X movement. *Plant Cell* **21**, 1541–55 (2009).
23. Jarsch, I. K. *et al.* Plasma Membranes Are Subcompartmentalized into a Plethora of Coexisting and Diverse Microdomains in Arabidopsis and Nicotiana benthamiana. *Plant Cell* **26**, 1698–1711 (2014).
24. Gronnier, J. *et al.* Regulation of immune receptor kinase plasma membrane nanoscale organization by a plant peptide hormone and its receptors. *Elife* **11**, (2022).
25. Ma, Z. *et al.* Membrane nanodomains modulate formin condensation for actin remodeling in Arabidopsis innate immune responses. *Plant Cell* **34**, 374–394 (2022).
26. Bücherl Christoph A Jarsch, I. K. *et al.* Plant immune and growth receptors share common signalling components but localise to distinct plasma membrane nanodomains. *Elife* **6**, 1–28 (2017).
27. Demir, F. *et al.* Arabidopsis nanodomain-delimited ABA signaling pathway regulates the anion channel SLAH3. *Proceedings of the National Academy of Sciences* **110**, 8296–8301 (2013).
28. Kleine-Vehn, J. *et al.* Recycling, clustering, and endocytosis jointly maintain PIN auxin carrier polarity at the plasma membrane. *Mol Syst Biol* **7**, 540 (2011).
29. Pinholt, H. D., Bohr, S. S. R., Iversen, J. F., Boomsma, W. & Hatzakis, N. S. Single-particle diffusional fingerprinting: A machine-learning framework for quantitative analysis of heterogeneous diffusion. *Proc Natl Acad Sci U S A* **118**, e2104624118 (2021).
30. Vítor, A. C. *et al.* Single-molecule imaging of transcription at damaged chromatin. *Sci Adv* **5**, (2019).
31. Hwang, D. W., Maekiniemi, A., Singer, R. H. & Sato, H. Real-time single-molecule imaging of transcriptional regulatory networks in living cells. *Nature Reviews Genetics 2024* 1–14 (2024) doi:10.1038/s41576-023-00684-9.
32. Obara, C. J. *et al.* Motion of VAPB molecules reveals ER–mitochondria contact site subdomains. **626**, (2024).
33. Murashige, T. & Skoog, F. A Revised Medium for Rapid Growth and Bio Assays with Tobacco Tissue Cultures. *Physiol Plant* **15**, 473–497 (1962).
34. Martinière, A. *et al.* Osmotic Stress Activates Two Reactive Oxygen Species Pathways with Distinct Effects on Protein Nanodomains and Diffusion. *Plant Physiol* **179**, 1581–1593 (2019).

35. Abel, N. B. *et al.* A hetero-oligomeric remorin-receptor complex regulates plant development Short title: A hetero-oligomeric remorin-receptor complex. *bioRxiv* 2021.01.28.428596 (2021) doi:10.1101/2021.01.28.428596.
36. Clough, S. J. & Bent, A. F. Floral dip: a simplified method for Agrobacterium -mediated transformation of Arabidopsis thaliana. *The Plant Journal* **16**, 735–743 (1998).
37. Marillonnet, S. *et al.* No Title. *Proc Natl Acad Sci U S A* **101**, 6852–6857 (2004).
38. Binder, A. *et al.* A Modular Plasmid Assembly Kit for Multigene Expression, Gene Silencing and Silencing Rescue in Plants. *PLoS One* **9**, e88218 (2014).
39. Ershov, D. *et al.* TrackMate 7: integrating state-of-the-art segmentation algorithms into tracking pipelines. *Nature Methods 2022 19:7* **19**, 829–832 (2022).
40. Schindelin, J. *et al.* Fiji: an open-source platform for biological-image analysis. *Nature Methods 2012 9:7* **9**, 676–682 (2012).
41. Jaqaman, K. *et al.* Robust single-particle tracking in live-cell time-lapse sequences. *Nat Methods* **5**, 695–702 (2008).
42. Saxton, M. J. & Jacobson, K. SINGLE-PARTICLE TRACKING:Applications to Membrane Dynamics. *https://doi.org/10.1146/annurev.biophys.26.1.373* **26**, 373–399 (2003).
43. Wallis, T. P. *et al.* Super-resolved trajectory-derived nanoclustering analysis using spatiotemporal indexing. *Nature Communications 2023 14:1* **14**, 1–16 (2023).

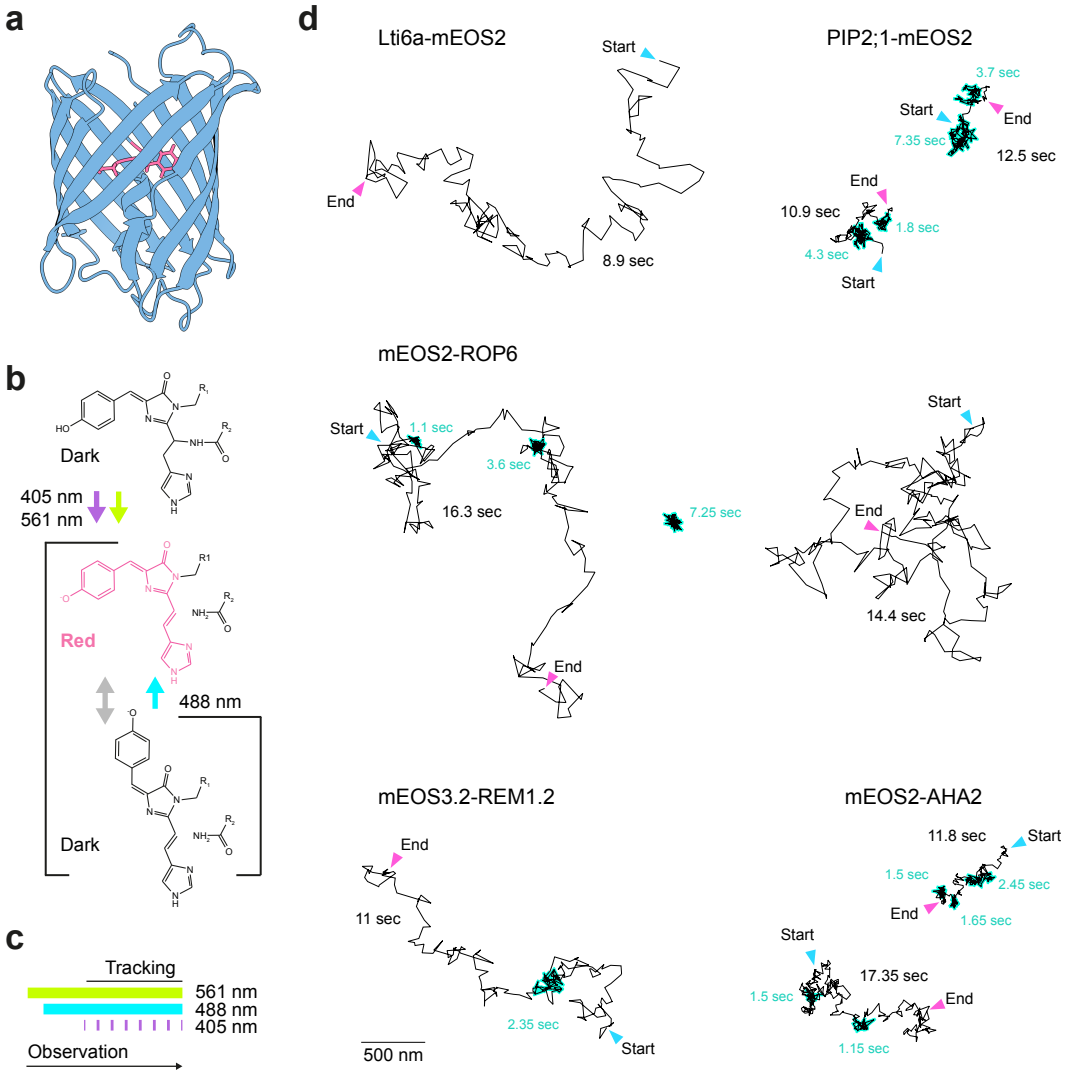

Figure 1 | Photochromic reversion enables long-term tracking of single molecules.

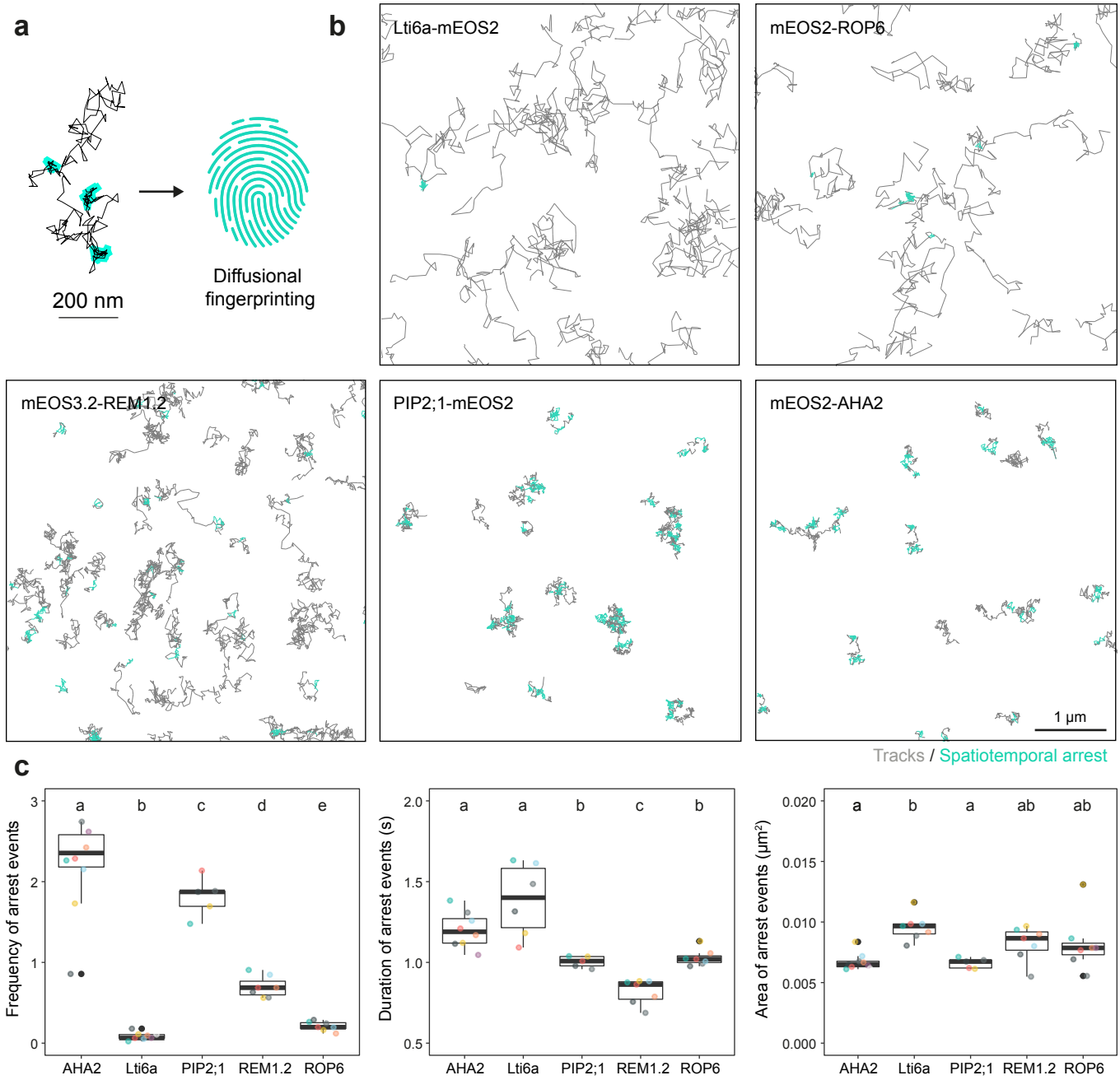

Figure 2 | Analysis of transient spatiotemporal arrest events of plasma membrane proteins.

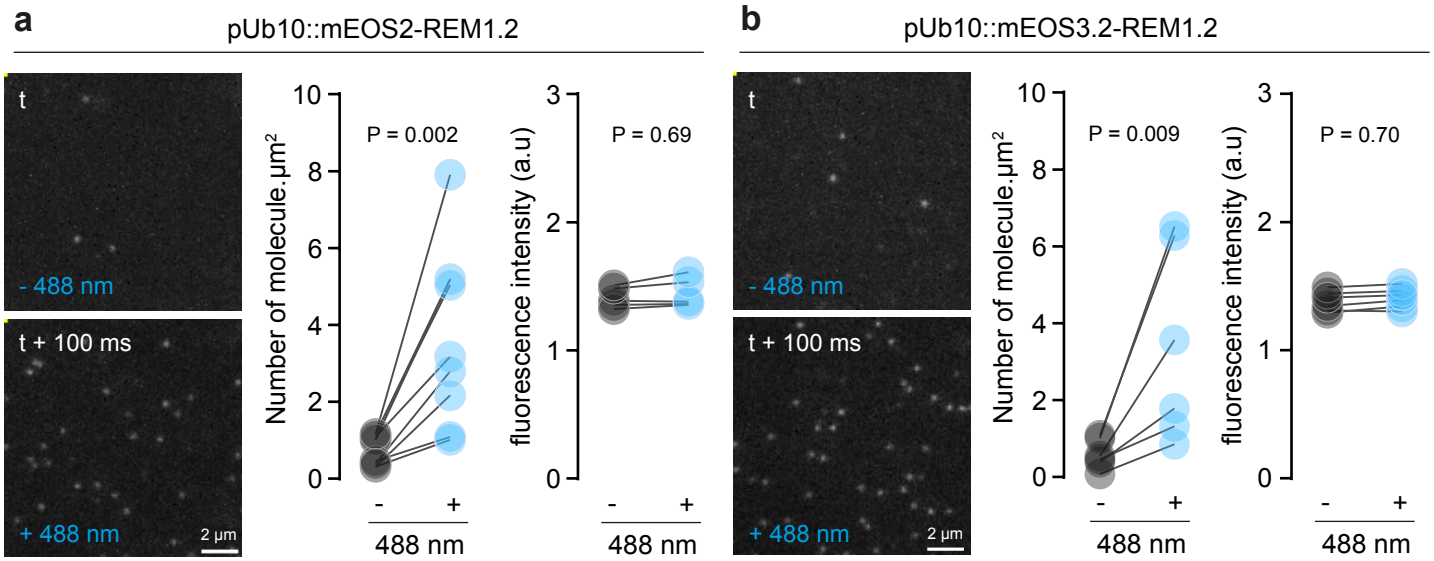

Supplementary Figure 1 | Effect of 488nm illumination on mEOS2-REM1.2 and mEOS3.2-REM1.2 molecules transiently expressed in N. benthamiana.

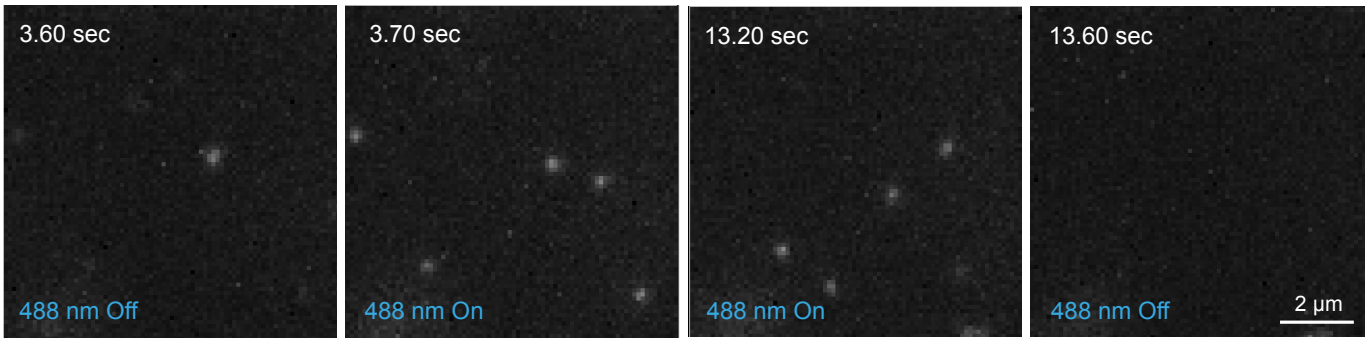

Supplementary Figure 2 | Single molecule rapidly return to a dark state in absence of 488 nm illumination.

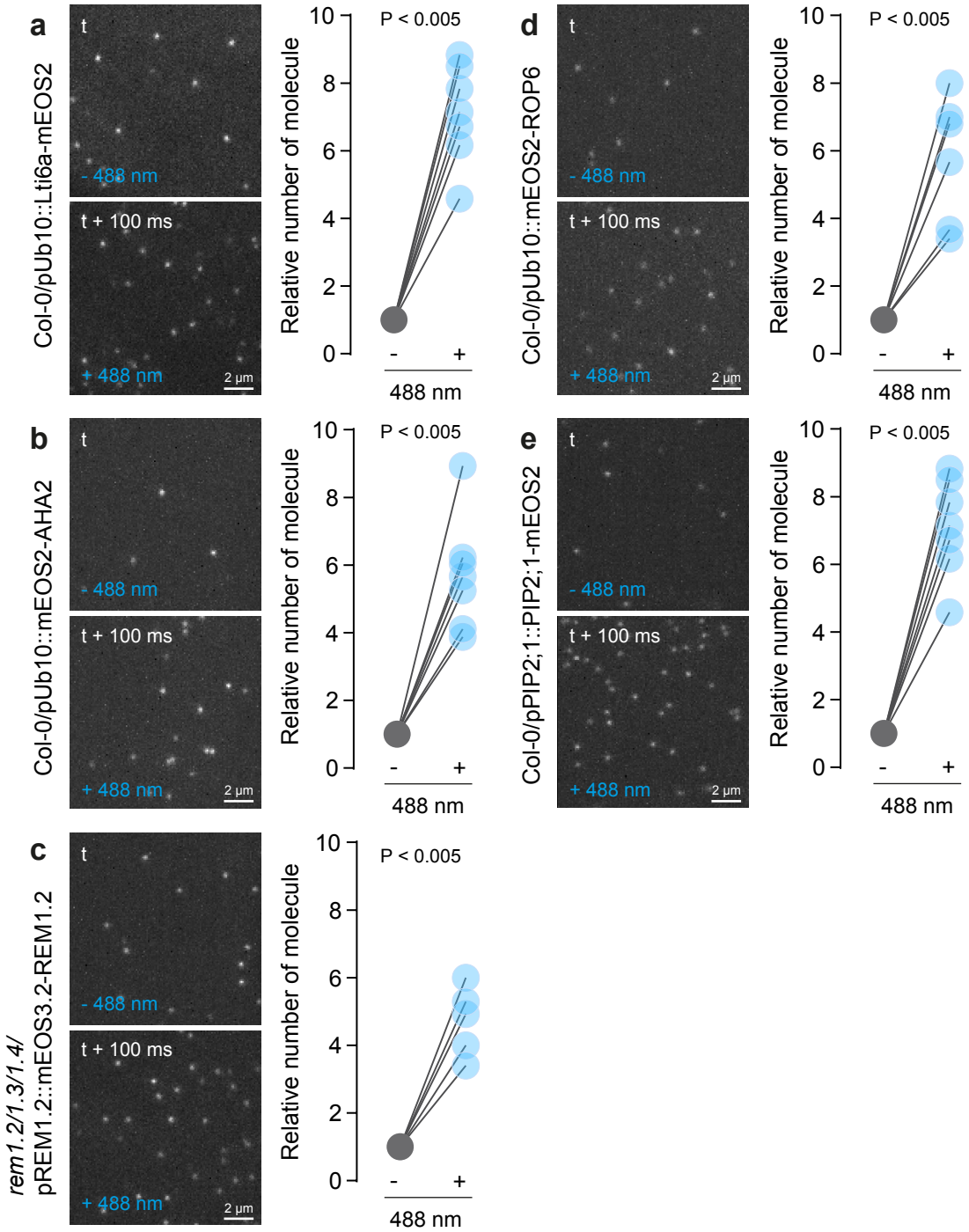

Supplementary Figure 3 | Effect of 488nm illumination on five plasma membrane-localized mEOS translational fusions expressed in Arabidopsis thaliana.

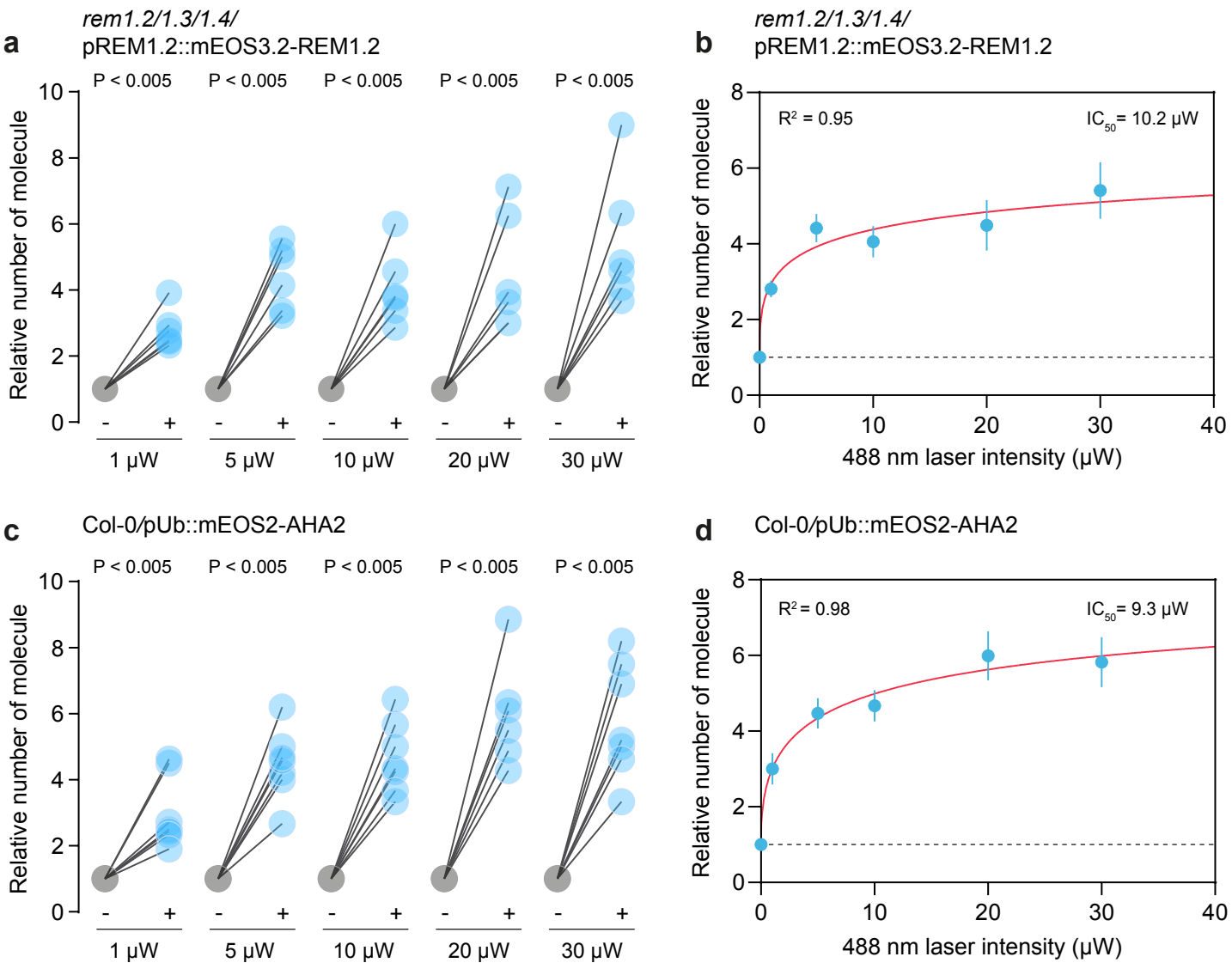

Supplementary Figure 4 | Analysis of the dose response to 488 nm light exposure.

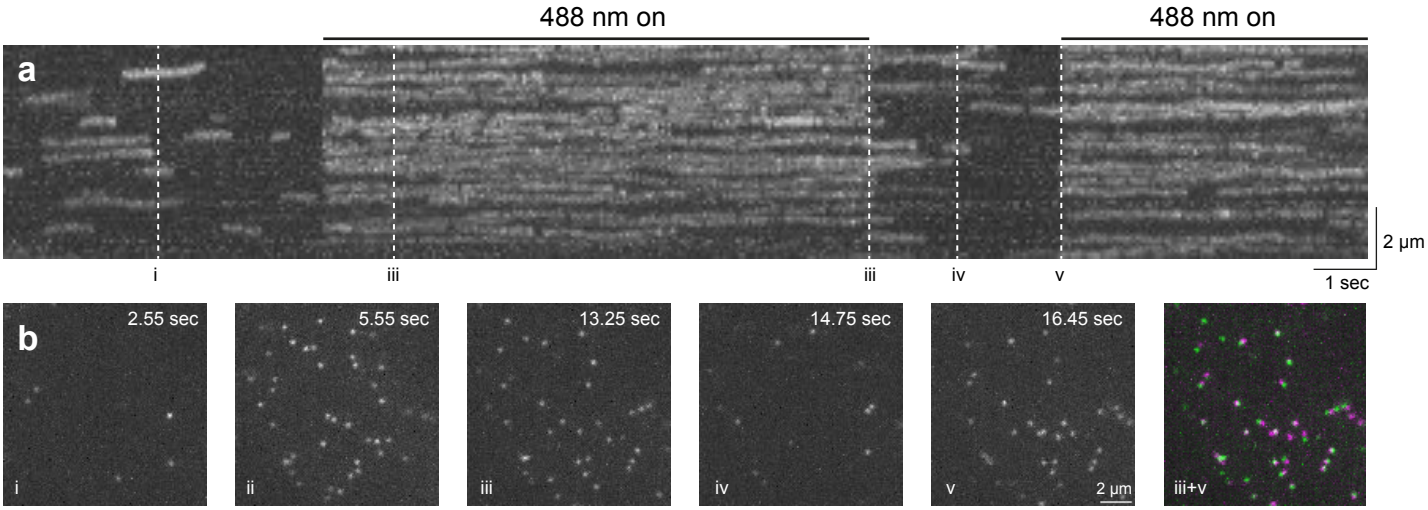

Supplementary Figure 5 | Sequential exposure to 488 nm shows controlled cycling of photo-converted mEOS molecules between fluorescent and dark state.

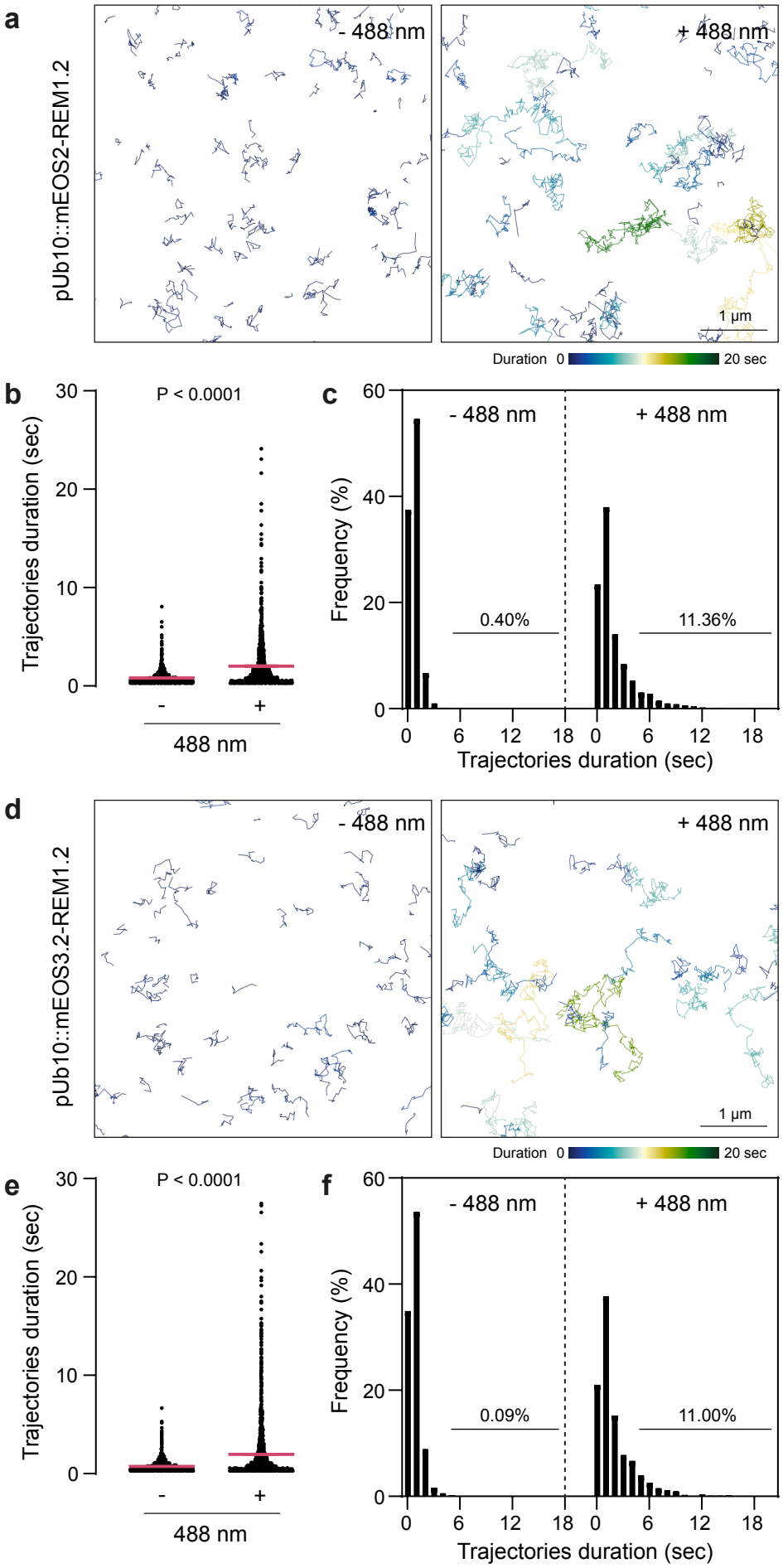

Supplementary Figure 6 | Effect of 488 nm light exposure on trajectories duration of mEOS2-REM1.2 and mEOS3.2-REM1.2 transiently expressed in N. benthamiana.

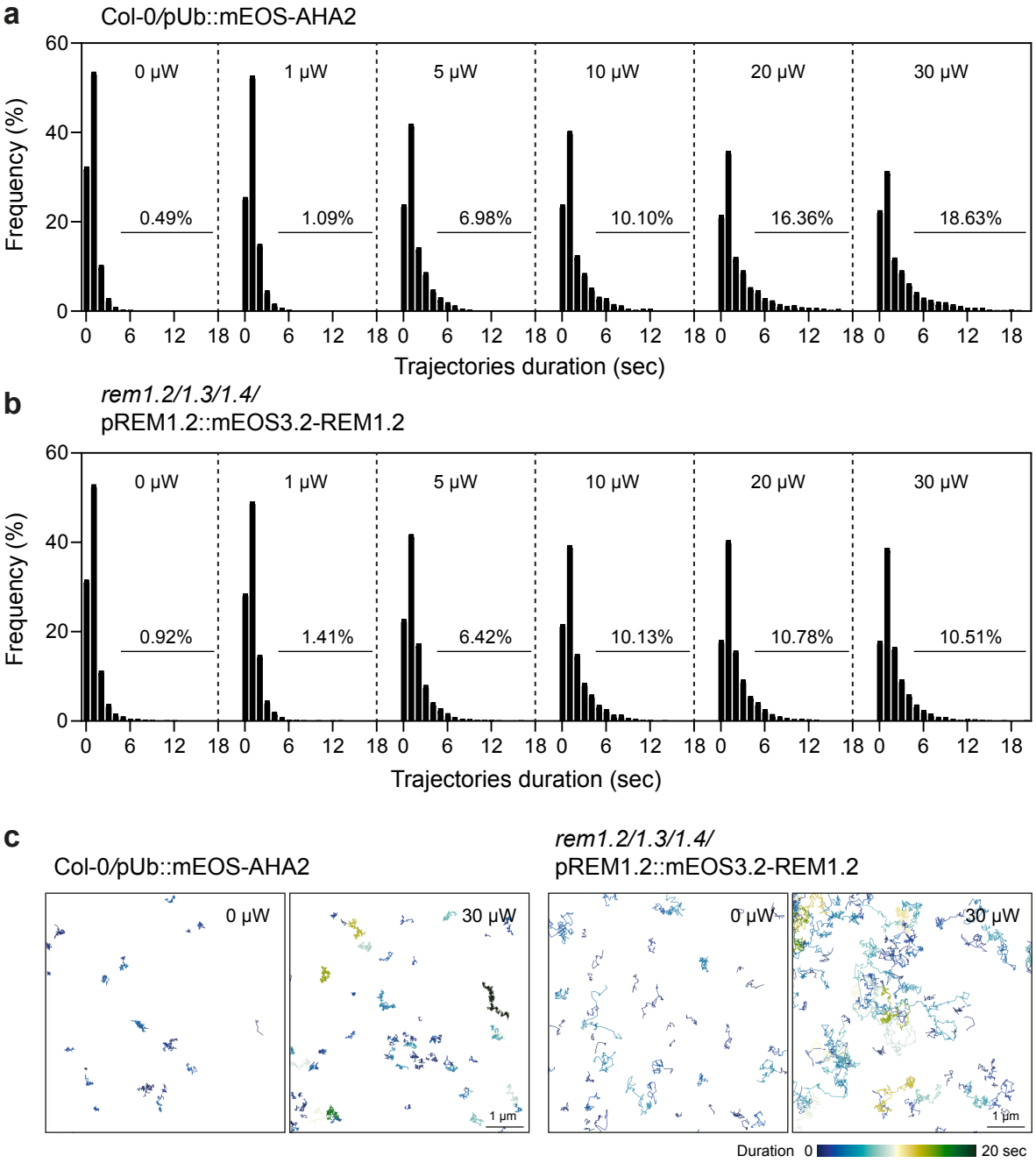

Supplementary Figure 7 | Effect of 488 nm light intensity on trajectories duration of mEOS2-AHA2 and mEOS3.2-REM1.2.

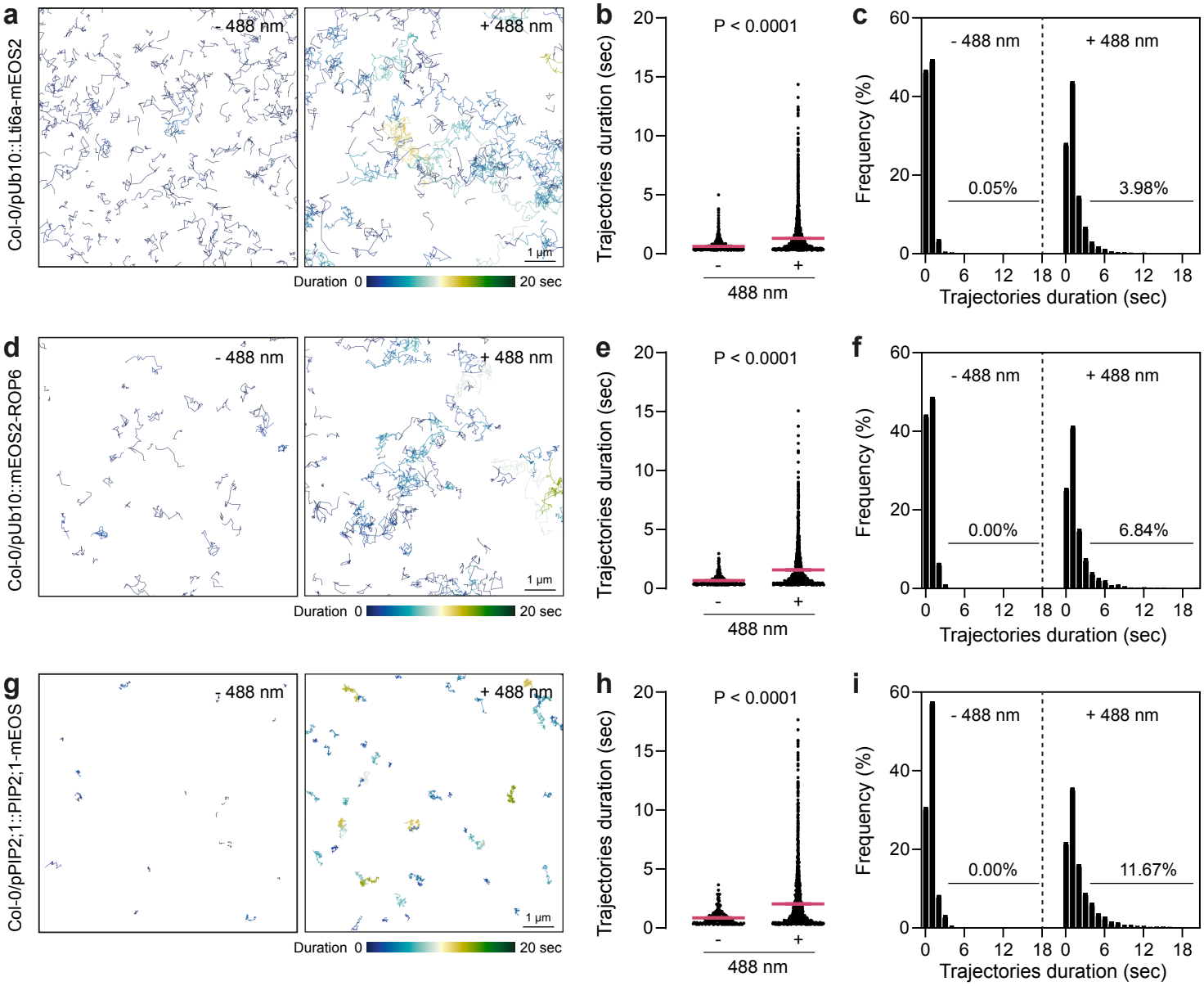

Supplementary Figure 8 | Effect of 488 nm light exposure on trajectories duration of Lti6a-mEOS2, mEOS2-ROP6 and PIP2;1-mEOS2.

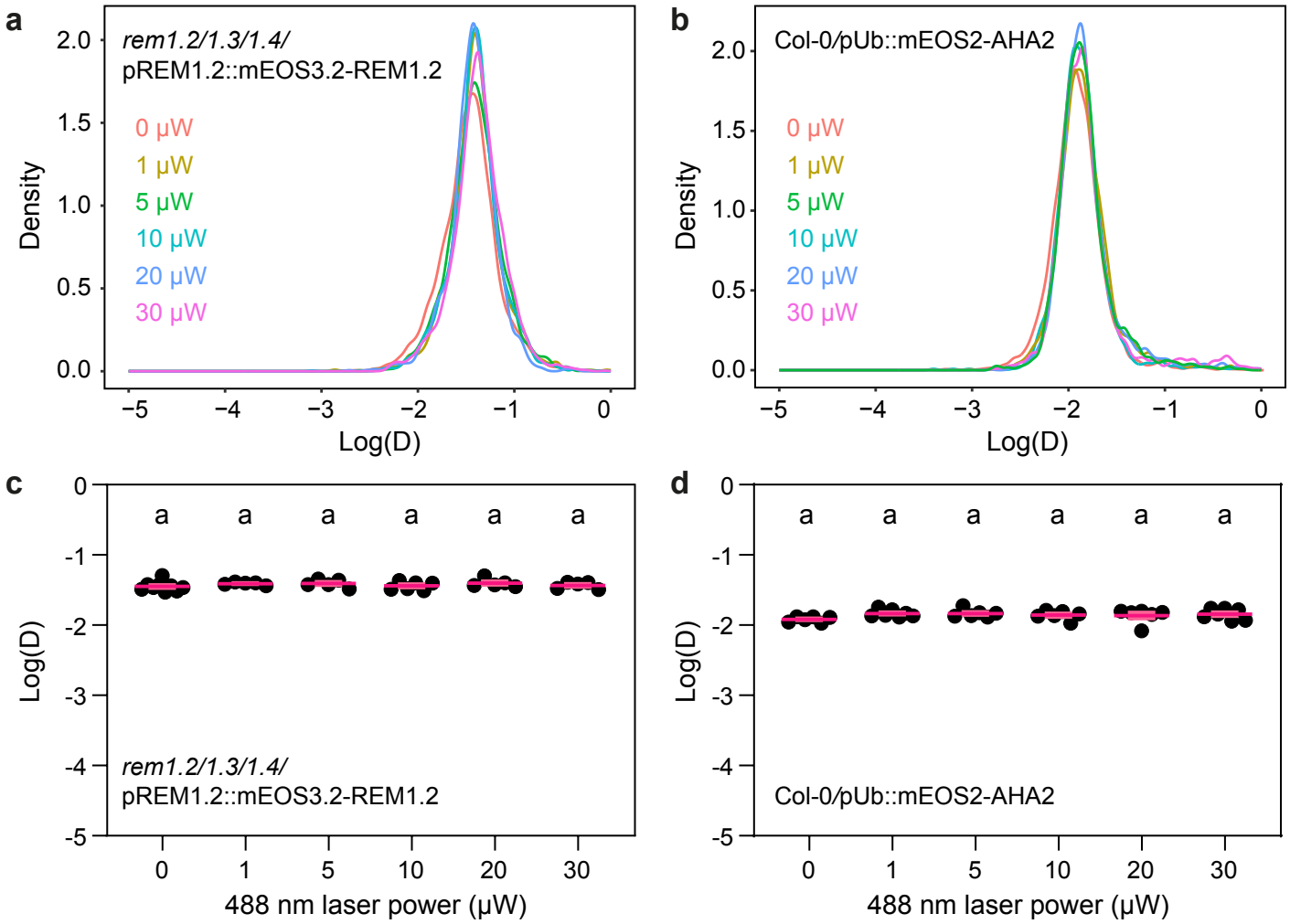

Supplementary Figure 9 | 488 nm light exposure does not affect diffusion coefficient.

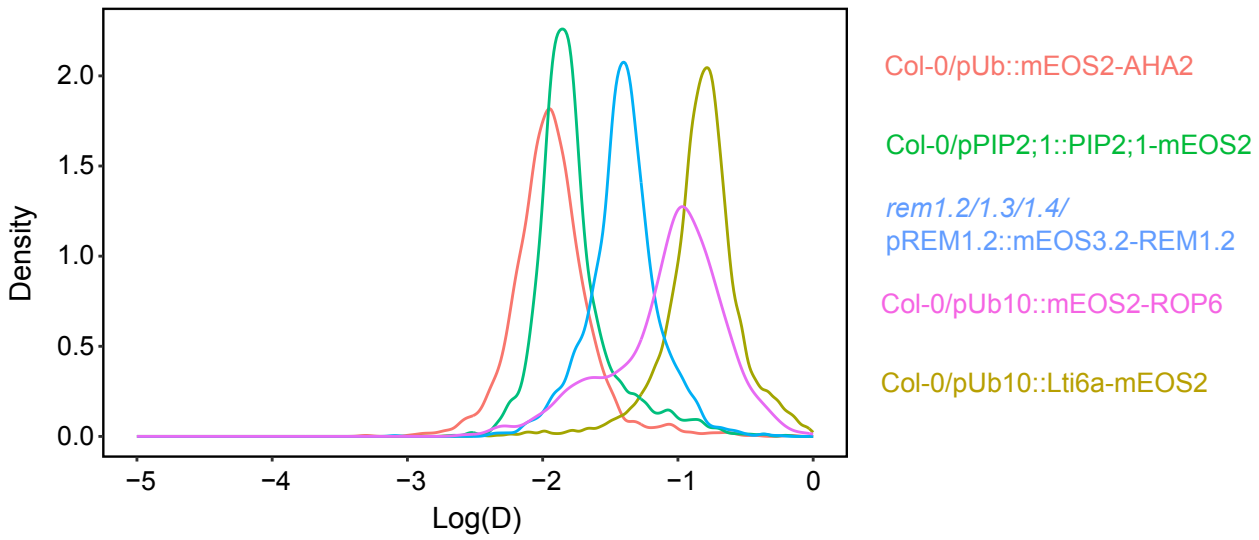

Supplementary Figure 10 | Analysis of the apparent diffusion coefficient of plasma membrane proteins used in this study.

rem1.2/1.3/1.4/
pREM1.2::mEOS3.2-REM1.2

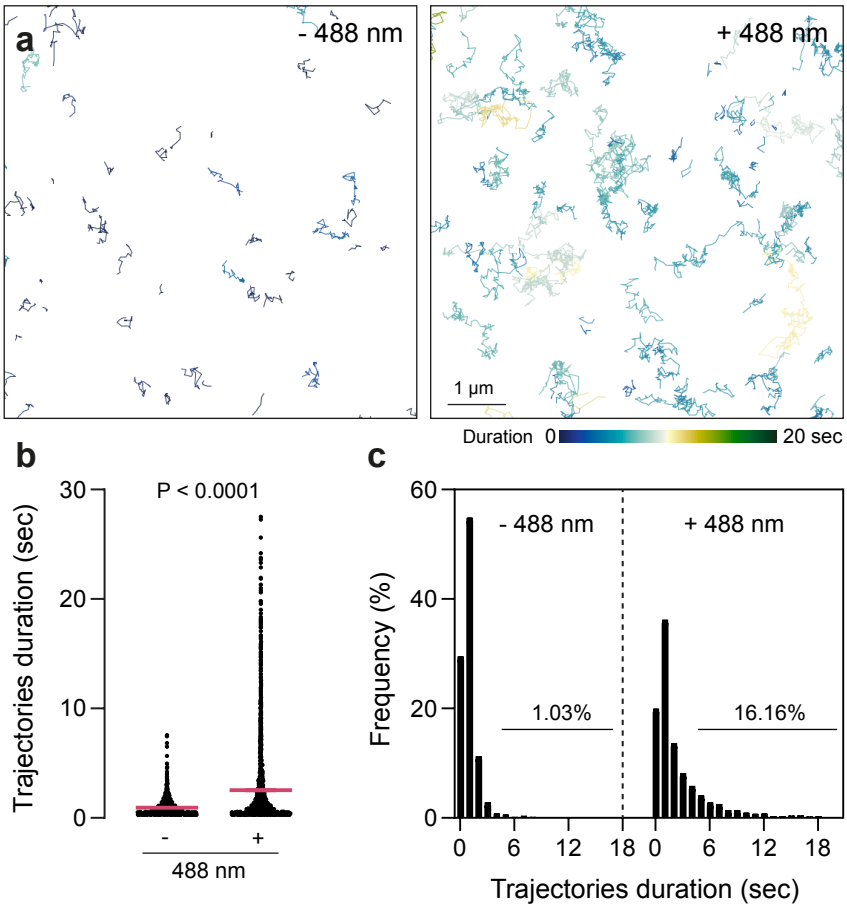

Supplementary Figure 11 | Analysis of trajectory duration of newly photo-converted molecules.

Supplementary Table 1 | List of primers used in this study.

Name	Sequences (5' to 3')
pAtREM1.2_A-B_BBO2-f	TTTGGTCTCAGCGGcgttgttattcatc
pAtREM1.2_A-B_BBO2-r	TTTGGTCTCACAGAagtcgccgcctc
AtREM1.2_C-D_BB02-f	TGGTCTCACACCATGGCGGAAGAACAGAAGATAGC
AtREM1.2_C-D_BB02_stop-r	TGGTCTCACCTTTCAGAAACATCCACAAGTTGCC